

Use of micromachined probes for the recording of cardiac electrograms in isolated heart tissues

Chang-Soo Kim^{a,1}, Stefan Ufer^b, Christopher M. Seagle^c, Connie L. Engle^c,
H. Troy Nagle^b, Timothy A. Johnson^c, Wayne E. Cascio^{c,*}

^a *Departments of Electrical & Computer Engineering and Biological Sciences, 1870 Miner Circle,
University of Missouri-Rolla, Rolla, MO 65409, USA*

^b *BioMedical MicroSensors Laboratory, Department of Electrical & Computer Engineering, North Carolina State University,
Raleigh, NC 27695-7911, USA*

^c *Division of Cardiology, Department of Medicine, University of North Carolina at Chapel Hill, Chapel Hill, NC 27599-7075, USA*

Received 19 February 2003; received in revised form 16 October 2003; accepted 30 October 2003

Abstract

Micromachined probes, with iridium (Ir) microelectrodes on silicon shanks, were evaluated to assess their suitability for cardiac electrogram recording. The electrochemical activation (anodic oxidation) procedure for the circular Ir microelectrode was investigated using the square wave potential according to the electrode size, number of cycles, and cathodic–anodic potential level of the square wave. Increase in the charge storage capacity was pronounced either in smaller electrodes or with higher potential level of the square wave. The electrode impedance reduced in a similar manner with increasing number of cycle irrespective of the electrode size. With either lower potential level ($-0.70/+0.60$ V) or smaller number of cycle (200 cycles) than those for the activation of stimulating electrode, the likelihood of overactivation of the recording microelectrode can be minimized. These anodic IrO_x film (AIROF) microelectrodes were used for the recording of extracellular electrograms in two different ex vivo cardiac tissue preparations. A single-shank microprobe was applied to the left ventricle of a mouse heart. Both the spontaneous and paced transmural responses propagating between epicardium and endocardium were obtained. Longitudinal cardiac wavefronts propagating along the rabbit papillary muscle were also recorded with a unique multiple-shank design. The measured mean amplitude and the propagation velocity of the extracellular voltage were 12.2 ± 1.8 mV and 58.9 ± 2.2 cm/s, respectively ($n = 27$). These microprobes with precisely defined electrode spacing make a useful tool for the spatial and temporal mapping of electrical properties in isolated heart tissues ex vivo.

© 2003 Elsevier B.V. All rights reserved.

Keywords: Iridium oxide; Microelectrode; Activation; Papillary muscle; Ventricle; Cardiac mapping

1. Introduction

Progress in solid-state microfabrication technologies has led the development of various types of integrated microelectrodes (Najafi, 1994). The most common use of these devices has been in neurological stimulation and recording applications, such as studies related to rehabilitative prosthesis and cognitive research. When applied to cardiac tissue, such microprobes hold promise as a means to

map extracellular voltage fields, characterize the resistive properties and define the sequence of electrical activation within small tissue preparations or small hearts such as the mouse.

Some pioneering attempts of cardiac recording with microfabricated probes in isolated hearts ex vivo have been reported. Multiple-electrode arrays fabricated on rigid and flexible substrates were developed for transmural cardiac recordings (Mastrototaro et al., 1992). Uni- and bi-polar recordings with these microprobes during normal sinus rhythm yielded recordings of similar quality to handmade probes. Linear and two-dimensional arrays of microelectrodes on a glass substrate were used to record multiple extracellular signals with high temporal and spatial resolution (Hofer et al., 1994). Activation patterns with a spatial

* Corresponding author. Tel.: +1-919-843-5217;
fax: +1-919-966-1743.

E-mail addresses: ckim@umr.edu (C.-S. Kim),
wayne_cascio@med.unc.edu (W.E. Cascio).

¹ Tel.: +1-573-341-4529; fax: +1-573-341-4532.

resolution within one cell length were measured at the surface of a papillary muscle to obtain a micromap of the spread of excitation.

We have been evaluating the suitability of micromachined silicon probes (Kléber et al., 1995; Smith et al., 1996), provided by the Center for Neural Communication Technology, University of Michigan (CNCT, 2003), for cardiac applications. These silicon microprobes have iridium (Ir) microelectrodes for the stimulation and the recording. Iridium oxide (IrO_x) layers can be grown on the surface of Ir electrodes by an electrochemical procedure (Robblee and Rose, 1990), thereby reducing the impedance and increasing the charge storage capacity of the electrode. This technique, known as the electrochemical activation procedure, has been well studied and optimized for maximal charge storage capacities during stimulation. However, we could not find a published activation protocol for recording applications for “smaller” passive recording microelectrodes. Thus, activation procedures of Ir for the recording purpose were systematically investigated with a variety of circular microelectrodes by different activation protocols.

We utilized two different microprobe designs. Single-shank microprobes as provided by CNCT were used in conjunction with a remote reference electrode to record the spatiotemporal sequence of transmural cardiac activation in isolated mouse hearts. A new multiple-shank microprobe was designed during this study and fabricated by CNCT for the purpose of measuring cardiac wavefronts propagating along the surface and intramural muscle layers of the isolated ventricular papillary muscle of the rabbit heart. With these microprobes, cardiac extracellular electrograms, for both spontaneous and paced responses, were obtained.

2. Materials and methods

2.1. Animal preparation and experimental setup

New Zealand white rabbits of either sex weighing 2–3 kg were heparinized (200 U/kg, IV) and euthanized with sodium pentobarbital (120 mg/kg, IV). Mice of either sex weighing 35–37 g were euthanized with sodium pentobarbital (120 mg, IP bolus). The animal preparation protocols and methodologies employed conformed to the guidelines advocated by the National Institutes of Health. A right ventricular papillary muscle and septum of the rabbit were isolated and perfused via the septal artery (Kléber and Riegger, 1987) with an erythrocyte-free perfusate composed of Tyrode’s solution (in mmol/l: Na^+ , 149; K^+ , 4.5; Mg^{2+} , 0.49; Ca^{2+} , 1.8; Cl^- , 133; HCO_3^- , 25; HPO_4^{2+} , 0.4; glucose, 20) plus insulin (1 U/l), heparin (400 U/l), albumin (2 g/l), and dextran (M_w : 70,000; 40 g/l). Likewise, the intact mouse heart was excised and perfused retrograde via the aorta. The time elapsed between cross clamping the aorta and perfusion was <5 min for both preparations. Once perfused, the rabbit septum or mouse heart was se-

cured in a lexan chamber, and the perfusate was delivered by a peristaltic pump. The preparations were enclosed in the chamber, surrounded by a humidified atmosphere and maintained between 36.5 and 37.5 °C. A membrane gas exchanger controlled the PO_2 and PCO_2 of the perfusate, and maintained the pH at 7.38. Perfusion pressure was recorded using a transducer (TCB-500, Millar) for both aortic and septal artery preparations; about 70 mmHg at flow rate of 1.5 ml/min both for mice and rabbits. The PCO_2 and PO_2 in the chamber were measured using a gas analyzer (Model 3750, Illinois Instruments) and were adjusted to match the values of the perfusate. A schematic representation of the experimental setup is provided in Fig. 1(a).

The microprobes are inserted into the arterially perfused papillary or isolated mouse heart as shown in Fig. 1(b). The mechanical strength of the silicon shank was satisfactory for cardiac applications. The microprobes are rigid enough for impaling the tissue, yet flexible enough for making recordings in an actively beating heart or tissue preparation. Other types of microprobe substrates made of rigid (molybdenum foil) or flexible (polyimide) materials (Mastrototaro et al.,

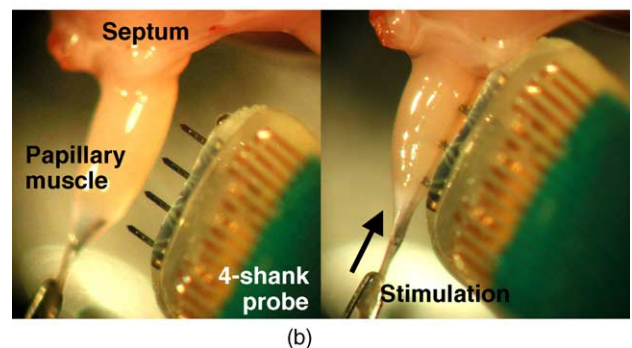
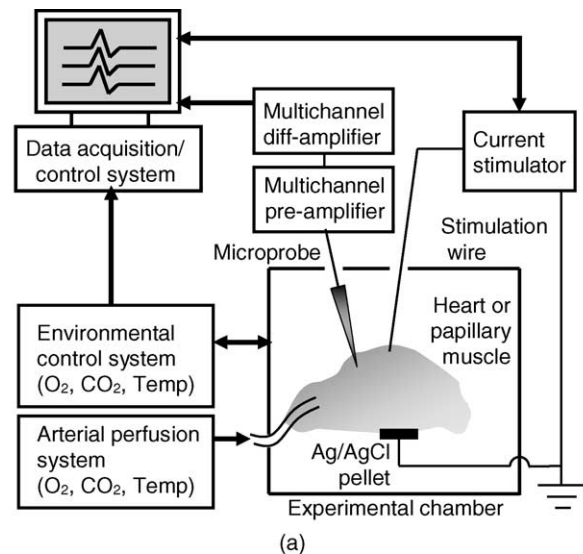


Fig. 1. Experimental setup. (a) The tissue preparation within a chamber with externally controlled environments and arterial perfusion; (b) A four-shank microprobe before (left) and after (right) insertion into the rabbit papillary muscle.

1992) can be alternatives to avoid the brittleness of the silicon microprobes. The silicon wafer, however, exhibits better standard processibility than metallic foils and does not need an additional cumbersome impaling apparatus to introduce the flexible microprobe into the tough cardiac tissue.

2.2. Micromachined probes

The single-shank design (Model 5 mm 100) with microelectrodes array provided by the CNCT was appropriate to study transmural cardiac activation in a small animal heart or isolated perfused cardiac tissue. This microprobe includes 16 circular Ir sites ($177 \mu\text{m}^2$) with spacings between 50 and $100 \mu\text{m}$ as shown in Fig. 2(a). A silk-wick reference electrode, Pt stimulating electrode, and Ag/AgCl pellet electrode (as the counter electrode for the stimulating electrode) were used in conjunction with this microprobe as shown in Fig. 1(a).

A second microprobe in Fig. 2(b) (Model four-shank-3) was specially designed in this study and fabricated by CNCT for recordings in the papillary muscle. Each shank has an array of three microelectrodes at different levels. A group of four microelectrodes in the same level on each shank represents one set of electrodes for activation measurements. Microelectrodes in the far left (or far right) shank can serve as reference electrodes for the other microelectrodes at the same level. This microprobe was employed to make multiple recordings of planar activation wavefronts propagating along the isolated papillary muscle by impaling the muscle perpendicular to its long-axis as shown in Fig. 1(b).

In addition to those microprobe designs, the Model three-shank-2 with $50 \mu\text{m}^2$ sites and the model passage with 413 and $1013 \mu\text{m}^2$ sites were also obtained. These larger Ir microelectrodes have been used to study the effect of electrochemical activation for biopotential recording sites over a range of areas of the Ir microelectrodes.

We have been using the microprobes for short-term recordings approximately up to 6 h. The microprobes are di-

rectly mounted and packaged on a rigid printed circuit board with a standard connector. The microprobe on the circuit board connector is plugged into a preamplifier held tightly by a micromanipulator. The micromanipulator is used to impale the microprobe into the papillary muscle or isolated mouse heart. During the experiment, the microprobe is held in a fixed position as the cardiac tissue beats.

2.3. Electrochemical activation of iridium microelectrodes

A three-electrode electrochemical setup was used to compensate solution resistance with the Ir microelectrode as the working electrode, a saturated calomel electrode (13-620-51, Fisher) as the reference electrode, and a platinum foil (+99.99%, Goodfellow) as the counter electrode. All electrodes were placed in an electrolytic solution of 0.3 M Na_2HPO_4 (Research grade, Alfa Chemicals). A potentiostat (IM6, BioAnalytical Systems) provided all electrochemical functions necessary for the electrochemical activation study, including ac impedance measurement, cyclic voltammetry, and controlled potential pulse operation.

Electrochemical activation waveforms were applied to the microelectrodes by the potentiostat in a controlled potential pulse mode and the resulting current was monitored. Square-wave cycling between a specified anodic and a cathodic potential level was used as the activation waveform. The impedance of the microelectrodes was determined using a 20 mV peak sinusoidal signal of various frequencies. For every microelectrode evaluation, the impedance spectrum and cyclic voltammogram were obtained before the electrochemical activation procedure was begun and after each consecutive activation step (50, 100, 200, 400, and 800 cycles). At each activation step, the cyclic voltammograms were performed only for one cycle with a scan rate of 100 mV/s at each activation step to minimize the contribution of cyclic voltammetry itself to the activation process.

2.4. Instrumentation

In the rabbit papillary muscle studies using micromachined silicon probes, we found that noise in our signals from the biopotential electrode sites was masking the characteristics of the extracellular electrograms. The noise components originated from two sources: stimulation artifacts and capacitive coupling in the lead wires. A preamplifier was constructed to minimize the effects of this noise (Andrews et al., 1994). This circuit used an operational amplifier (Burr-Brown OPA 404) in a voltage follower configuration, which was chosen specifically for its high input impedance ($10^{14} \Omega$ in parallel with 3 pF) relative to the output impedance of the microelectrode sites. Its high input and low output impedance minimizes the noise effects due to capacitive coupling. Input voltage clamping using a diode (National Semiconductor JFET 2N4117A) between the non-inverting input of the amplifier and a fixed reference potential (-3 V) prevented saturation of the amplifier

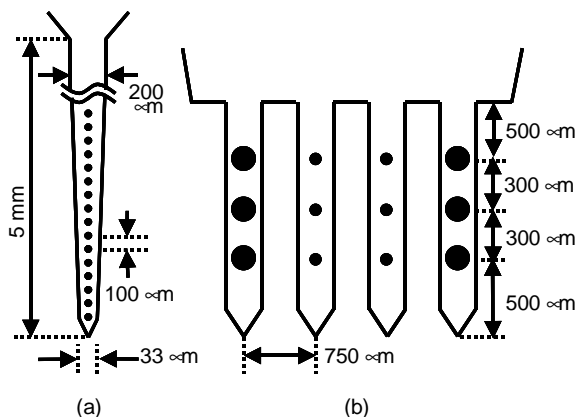


Fig. 2. Two microprobe designs used in papillary muscle experiments. (a) Model 5 mm 100 with $177 \mu\text{m}^2$ circular iridium sites; (b) Model four-shank-3 with 133 and $3847 \mu\text{m}^2$ circular iridium sites.

during the delivery of the stimulation pulse. In this way, the noise effects due to the stimulation artifact were minimized. Signals from the microprobe and reference electrodes were differentially amplified (an additional reference electrode has been used in case of the single-shank microprobe experiment). Current stimulation was controlled by the data acquisition/control system as shown in Fig. 1(a).

Data were collected on a Dell Pentium III PC running Windows ME using a National Instruments AT-MIO16E1 analog-to-digital converter. Custom software (*flexiDAQ*TM v1.7 written using National Instruments LabWindows/CVITM v5.5 in concert with NI-DAQTM v6.8) was used to direct the digitization of 16 data channels (10 K samples/s with 2 s duration). Sub-threshold (5 μ A with 20 ms duration) and threshold (150–500 μ A with 2 ms duration) stimulation pulses, separated by 20 ms, were delivered at a rate of 2–4 Hz using a WPI Linear Stimulus Isolator A395 driven by *flexiDAQ*TM D-to-A commands.

3. Results and discussion

3.1. Characterization of iridium microelectrodes

The basic electrochemical activation scheme recommended by the University of Michigan was adopted as the starting condition for this study (CNCT): 1 Hz square wave, cycling the potential between -0.85 and $+0.75$ V versus saturated calomel electrode (SCE), for approximately 600 cycles in 0.3 M Na_2HPO_4 solution. This procedure was developed for activating stimulating electrodes with relatively large areas for large charge storage capacity. This activation process can also be applicable to decrease the microelectrode impedance for recording applications.

Several variations of the square wave (frequency, anodic–cathodic potential level, and number of activation cycles) were considered to determine an optimal activation procedure for small recording microelectrodes. Two previous reports described the dependence of activation rate on the frequency. In a triangular activation mode (Buckley et al., 1976), the charge capacity after activation with the waveforms in the range of 0.1–10 Hz did not exhibit a substantial change. However, an increase in the oxide growth rate (in terms of anodic current peak in the voltammogram) was reported with respect to square-wave frequencies between 0.1 and 2 Hz (Vukovic, 1987). Therefore, all experiments were done at an intermediate frequency of 1 Hz in our study.

The effect of cathodic and anodic potential levels on Ir disc electrodes have been investigated as well (Bock and Birss, 1999; Buckley et al., 1976; Burke and Scannell, 1984; Gottesfeld and McIntyre, 1979; Zerbino et al., 1978). Low potential levels in both polarities do not contribute to the oxide growth. Increasing the cathodic (making it more negative) and the anodic (making it more positive) potentials accelerates the rate of oxide growth. Energetic gas evolu-

tion, however, at potential levels beyond the water electrolysis window leads to a rapid increase of current, which may cause delamination of the IrO_x layer. The activation potential for the microprobes provided by the University of Michigan was determined to be optimum ($-0.85/+0.75$ V) just inside the water electrolysis window for the stimulating application (CNCT). In our voltammetric study, abrupt increases of currents at both extremes of the applied potential levels were observed occasionally. This phenomenon was avoided by decreasing the potential to lower values ($-0.70/+0.60$ V). Fig. 3(a) shows a lower degree of oxide activation (area under the traces) at reduced potential levels. With this procedure, occasional cracking on the microelectrode surface was not found.

Charge storage capacities of different microelectrode areas activated with this procedure are plotted in Fig. 3(b). The densities of positive and negative charge storage capacity (the integral area under positive and negative current traces of the cyclic voltammogram, respectively) of smaller

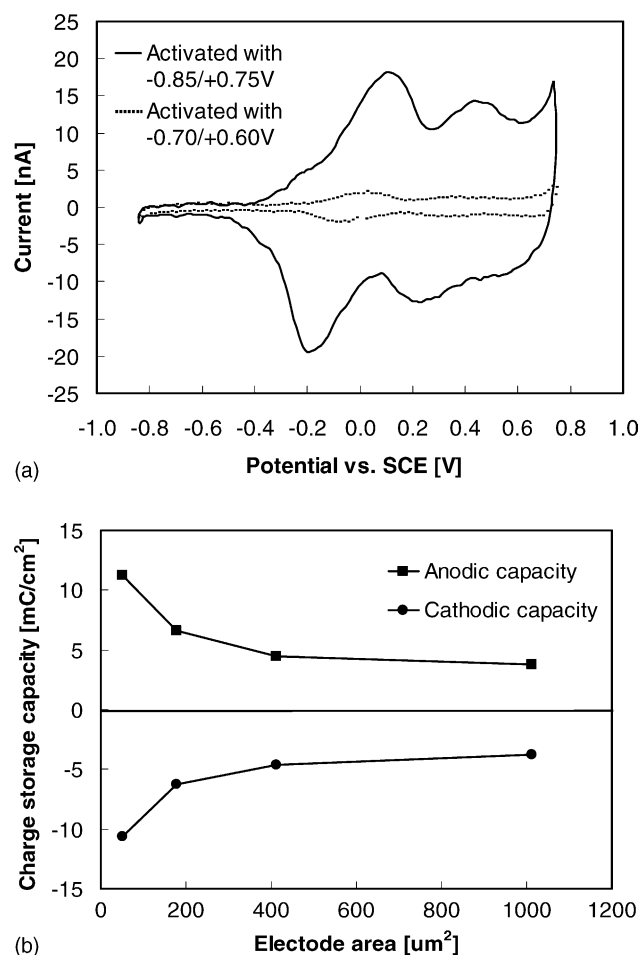
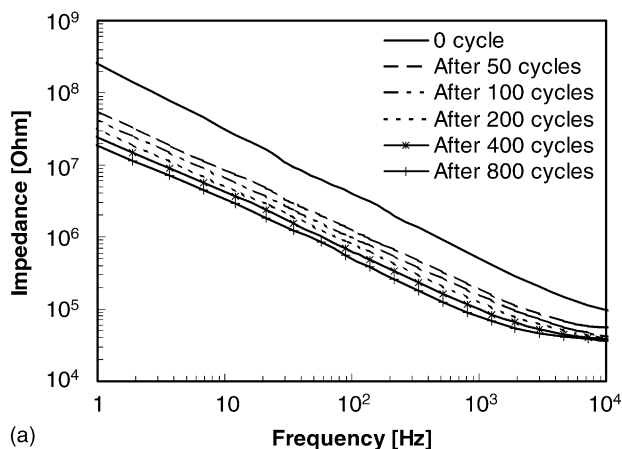


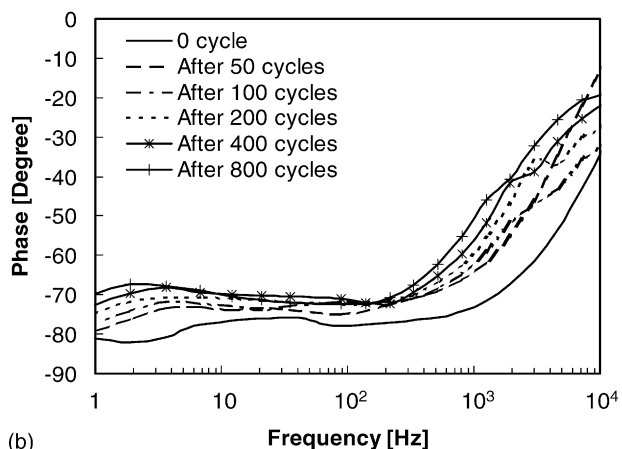
Fig. 3. Effect of potential levels and electrode area on the electrochemical activation of iridium oxide. (a) Cyclic voltammogram of iridium oxide with different cathodic–anodic potential levels (177 μm^2 electrodes; after 800 activation cycles); (b) effect of electrode area on charge storage capacity (after 800 activation cycles; potential level $-0.70/+0.60$ V).

electrodes are higher than those of larger electrode. In circular microelectrode, the flux of electrochemical species reacting at the surface is not uniform and a hemispherical diffusion layer can be envisioned over the entire electrode surface (Wightman and Wipf, 1989). This convergent diffusion behavior is due to the edge effect in which a significant portion of the electrochemical reaction takes place at its circumference. This fact is supported by the behavior of ring electrodes that is a similar configuration with a circular electrode from which a central portion of less use was eliminated (Wightman and Wipf, 1989). Therefore, it is considered that a lower form factor (i.e. the circumference to enclosed area ratio) of larger microelectrode caused a lower density of charge storage capacity.

Fig. 4(a) and (b) show impedance and phase spectra of a $177 \mu\text{m}^2$ electrode activated with cathodic–anodic potential levels of $-0.70/+0.60 \text{ V}$. In both cases, the effect of the first 50 cycles is most pronounced. The impedance decreases as the number of activation cycles increases. The impedance continues to decrease as the activation proceeds beyond 50 cycles, but at a much slower rate, eventually reaching a min-



(a)



(b)

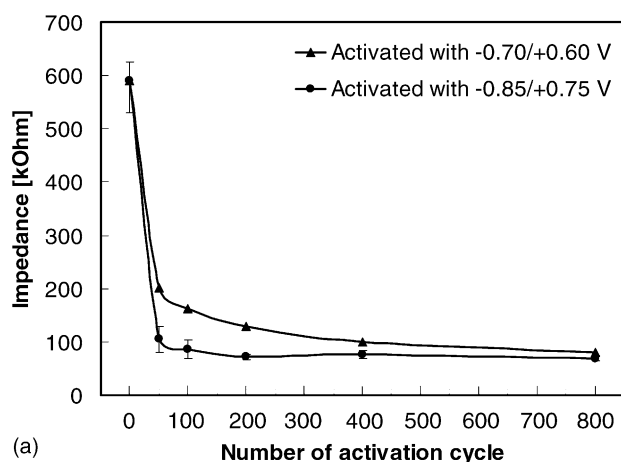
Fig. 4. Reduction of electrode impedance and increase of charge storage capacity with consecutive activation cycles. (a) Impedance and (b) phase spectra with consecutive activation cycles ($177 \mu\text{m}^2$ electrode; potential level $-0.70/+0.60 \text{ V}$).

imum value in an exponential manner. This type of evaluation was performed on various circular microelectrodes, with electrode areas between 50 and $1013 \mu\text{m}^2$. The first 50 cycles of activation appear to have the largest effect on microelectrode impedance, irrespective of the electrode area.

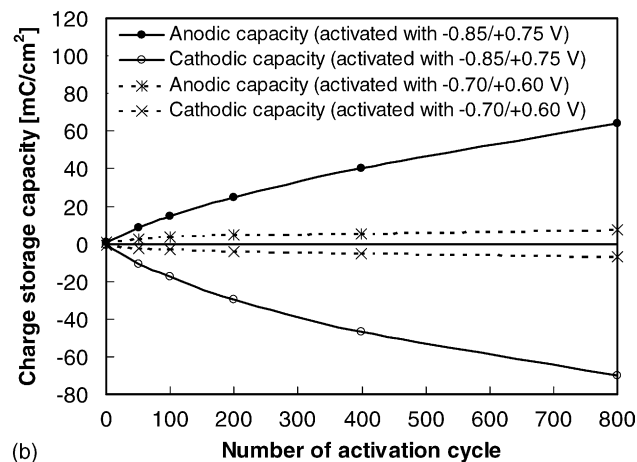
Fig. 5(a) illustrates the relationship between the activation potentials and microelectrode impedance at 1 kHz and the charge storage capacity of $177 \mu\text{m}^2$ electrodes. There are initial steep decreases in impedance during the first 50 cycles of activation in both cases. An increase in charge storage capacities can be observed with respect to the number of activation cycles as shown in Fig. 5(b). Changes in electrode impedance and charge capacity are much more pronounced for higher potential levels, which is also apparent from Fig. 3(a).

3.2. Extracellular cardiac electrograms

The shape and amplitude of recorded extracellular potential are affected by the electrical coupling between tissue and electrode. During the ex vivo use of microprobe, the interface of tissue and IrO_x can be varied probably



(a)



(b)

Fig. 5. Effect of potential level on: (a) electrode impedance at 1 kHz ; and (b) corresponding charge storage capacity ($177 \mu\text{m}^2$ electrodes).

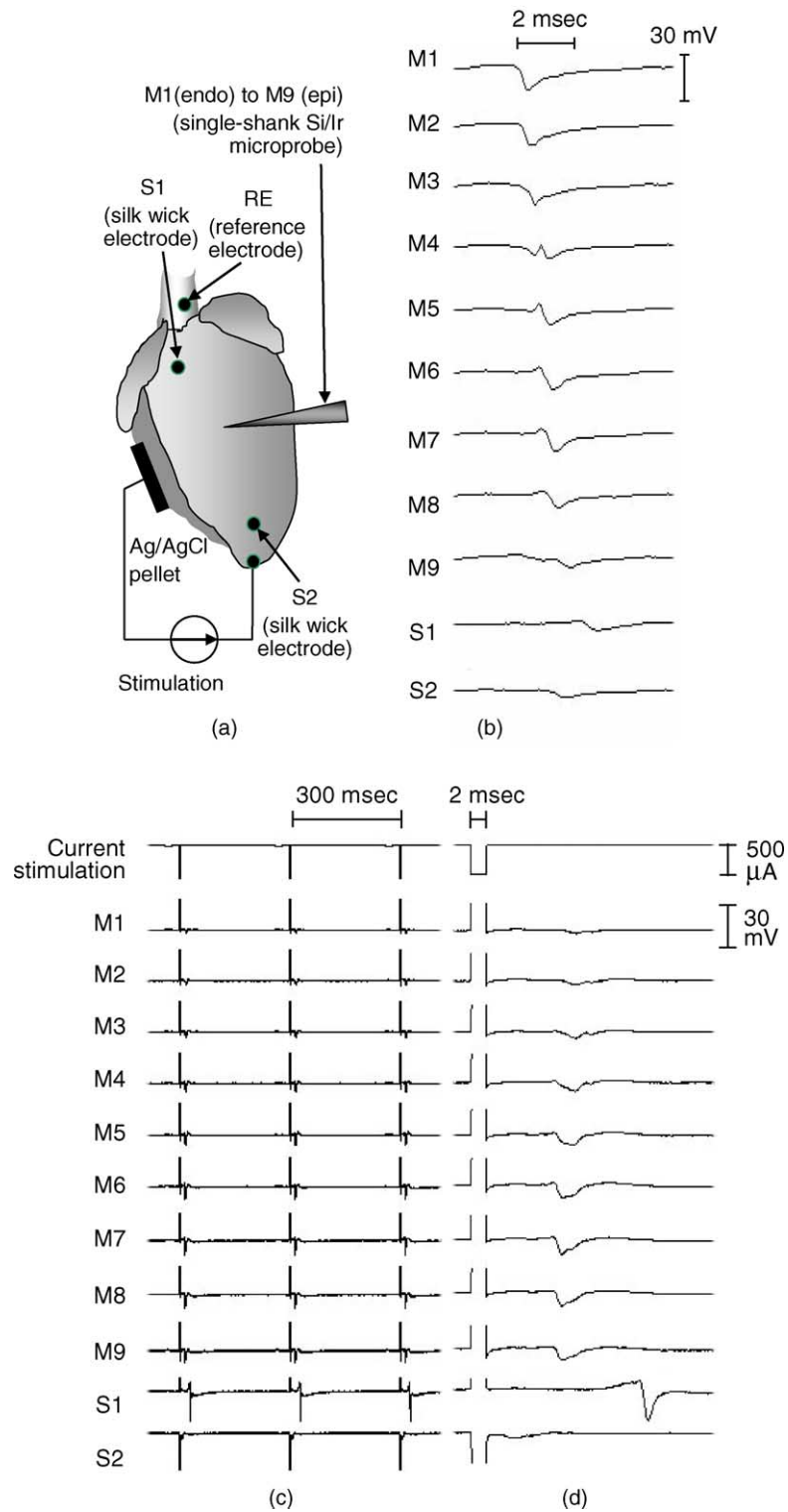


Fig. 6. Recording of transmural cardiac activation with the 16-channel single-shank microprobe in the left ventricle of a mouse heart. (a) Location of the electrodes in the preparation; (b) spontaneous transmural cardiac activation (M1 \rightarrow M9 \rightarrow S2 \rightarrow S1); (c) stimulation artifacts and paced transmural cardiac activation (S2 \rightarrow M9 \rightarrow M1 \rightarrow S1); (d) an expanded view of one activation signal in (c).

due to absorption of proteins or other biomolecules. The exposure of the electrode surface to undefined body fluid makes the change of impedance unpredictable. According to an impedance model developed for the IrO_x stimulation electrode (Weiland and Anderson, 2000), the roughness and porosity of IrO_x surface further contribute to complex and non-uniform frequency-dependent impedance. Therefore, quantitative interpretations of recorded cardiac signals with respect to a universally valid microelectrode impedance model have yet to be firmly established (Connolly et al., 1990). Under any circumstances, however, a recording electrode should be prepared to have the minimum impedance at a given geometry for high quality recordings.

The electrochemical activation of Ir microelectrode simultaneously decreases the electrode impedance and increases the charge storage capacity of the electrode. For the recording microelectrode low impedance is of primary concern, rather than the high charge storage capacity which is the critical factor in stimulating electrode. Therefore, in this study, the microelectrode impedance was controlled by one of two different activation procedures (see Fig. 5(a); cycles with potential level of $-0.85/+0.70$ V, or 400 cycles with $-0.70/+0.60$ V versus SCE in a 0.3 M Na_2HPO_4 solution), which allows us to achieve maximum reduction in the impedance with minimum electrochemical activation.

The usability and functionality of the single-shank microprobe in cardiac application was first tested by recording of the spontaneous transmural cardiac electrograms. Fig. 6(a) shows the location of the electrodes in the mouse heart. A silk-wick reference electrode (RE) was placed on the aortic root. Two other silk-wick electrodes were placed to record the spontaneous electrograms at the basal and apical left ventricle for comparison with those recorded from the microprobe. Fig. 6(b) shows spontaneous transmural cardiac electrograms in the left ventricle obtained with a single-shank microprobe. Multiple electrograms from the microelectrodes at the middle of the left ventricle and two silk-wick electrodes exhibit a normal sequence of activation from the atrium to the ventricle. In the ventricle activation of the mouse ventricle proceeds from the endocardium (M1) to epicardium (M9) as it does in the human heart (Durrer et al., 1970).

An electrode pair of a platinum stimulation wire and a Ag/AgCl pellet were introduced to produce paced electrograms as shown in Fig. 6(a). During unipolar left ventricular pacing near the left ventricular apex, local unipolar electrograms are recorded as shown in Fig. 6(c). After each stimulation artifact caused by the pacing signal (500 μA with 2 ms duration), cardiac activation signals are recorded in each channel. Fig. 6(d), an expanded time scale of one activation signal in Fig. 6(c), shows a sequence of left ventricular and transmural activation. Propagation proceeds from the apex (S2) to the basal left ventricle (S1), and from the epicardium (M9) to the endocardium (M1), which takes about 24 and 2 ms, respectively.

The four-shank microprobe was used to record longitudinal wavefronts of a rabbit papillary muscle in response to sub-threshold current injection. In the isolated perfused papillary muscle, sub-threshold current (10 μA with 20 ms duration) and supra-threshold current (200 μA with 2 ms duration) were injected at the tendonous end of the muscle. The stimulation waveforms and the resulting responses are shown in Fig. 7(a). The amplitude of voltage response to sub-threshold stimulation is proportional to the distance between the recording electrodes and the reference electrode. An expanded view in Fig. 7(b) shows longitudinal propagation of the activation signal along the papillary muscle. As presented in Fig. 7(c), the three microelectrodes in the proximal shank to the septum served as reference electrodes (RE), each for the microelectrodes of the same depth in other shanks. The mean amplitude of the measured extracellular voltages by nine microelectrodes during the three consecutive supra-threshold stimulations was 12.2 ± 1.8 mV ($n = 27$). The propagation velocity estimated from the time

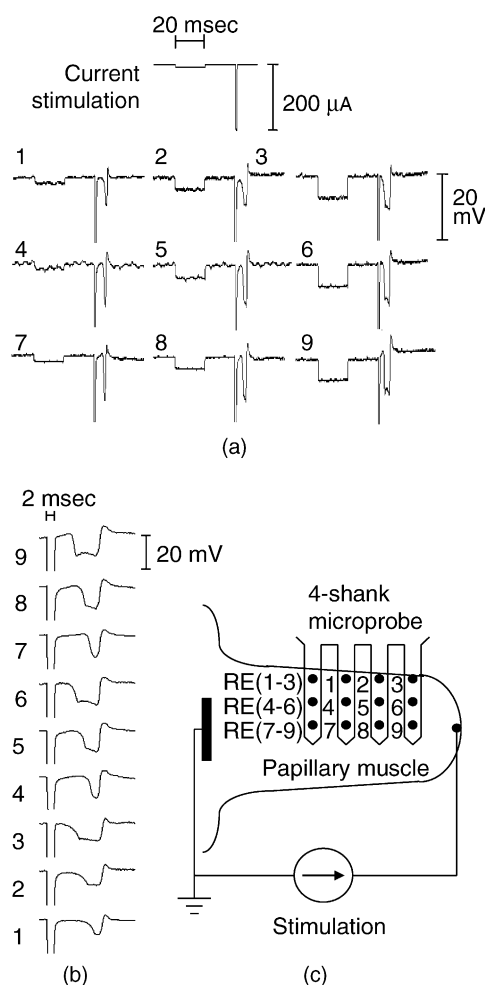


Fig. 7. Recording of longitudinal cardiac wavefronts and sub-threshold signals with the four-shank microprobe in the rabbit papillary muscle. (a) Sub-threshold responses and paced electrograms; (b) an expanded view of paced electrograms in (a); (c) location of the electrodes in the preparation.

interval between the onset of supra-threshold stimulation and the maximum negative slope of extracellular voltage activation was 58.9 ± 2.2 cm/s ($n = 27$), which is consistent with the reported value of 57 cm/s (Kléber and Riegger, 1987). It is expected that the shape of cardiac wavefront in the papillary muscle according to the depth can be identified with much refined microprobe design.

One limitation of the microprobe is that some relative motion between the microelectrode and the surrounding cardiac tissue can be present depending on the position of the microprobe and the vigor of tissue contraction. A future improvement in the experimental method will incorporate a flexible cable between the microprobe and the circuit board connector to minimize the effect of cardiac tissue movement. We further envision the utility of the four-shank microprobe we designed in this study for application to the microscale tissue impedance measurements. The larger electrodes in the pair of outer shank may be used as the current injecting electrodes and their counter electrodes in the 4-point impedance measurements. The electrodes in the pair of inner shank can then be used for the recording electrodes and reference electrodes.

4. Conclusion

The proposed electrochemical activation procedure, with either lower potential level or smaller number of cycle than those for the activation of stimulating electrode, the likelihood of overactivation of the recording microelectrode can be minimized. The microprobes utilized in this study provided advantages to perform two important cardiac physiological experiments. First, the 16-channel single-shank microprobe was able to record the sequence of transmural electrical activation in the mouse heart. Second, the four-shank microprobe is capable of measuring longitudinal electrical activation and extracellular voltage distributions in the isolated arterially perfused papillary muscle in a well-defined spatial distribution. These microprobes with precisely defined electrode spacing are an useful tool for advanced spatial and temporal recordings of extracellular voltage profiles in isolated cardiac tissues *ex vivo*. A quantitative analysis of the correlation of the obtained electrogram and the microelectrode impedance requires more information for the modeling of the tissue- IrO_x interface and complex real tissue environment surrounding a microelectrode.

Acknowledgements

The studies were supported by P01 HL27430 from the National Institutes of Health; Heart, Lung and Blood Institute, Bethesda, MD, USA. The authors thank Dr. Kenneth Wise, Dr. David Anderson and Ms. Jamie Hetke for providing micromachined probes fabricated by the Center for

Neural Communication Technology, University of Michigan sponsored by NIH/NCRR Grant P41-RR09754.

References

- Andrews, C.A., Kermani, B.G., Cascio, W.E., Nagle, H.T., 1994. Controlling electrical side effects of cardiac stimulus pulses due to high impedance electrodes. In: Proceedings of the 16th Annual International Conference of the IEEE Engineering in Medicine and Biology Society (on CD-ROM).
- Bock, C., Birss, V.I., 1999. Irreversible decrease of Ir oxide film redox kinetics. *J. Electrochem. Soc.* 146, 1766–1772.
- Buckley, D.N., Burke, L.D., Mulcahy, J.K., 1976. The oxygen electrode. Part 7. Influence of some electrical and electrolyte variables on the charge capacity of iridium in the anodic region. *J. Chem. Soc., Faraday I* 72, 1896–1902.
- Burke, L.D., Scannell, R.A., 1984. An investigation of hydrous oxide growth on iridium in base. *J. Electroanal. Chem.* 175, 119–141.
- CNCT, 2003. Website of the Center for Neural Communication Technology (CNCT), University of Michigan (<http://www.engin.umich.edu/facility/cnct>).
- Connolly, P., Clark, P., Curtis, A.S.G., Dow, J.A.T., Wilkinson, C.D.W., 1990. An extracellular microelectrode array for monitoring electrogenic cells in culture. *Biosens. Bioelectron.* 5, 223–234.
- Durrer, D., van Dam, R.T., Freud, G.E., Janse, M.J., Meijler, F.L., Arzbaeher, R.C., 1970. Total excitation of the isolated human heart. *Circulation* 41, 899–912.
- Gottesfeld, S., McIntyre, J.D.E., 1979. Electrochromism in anodic iridium oxide films. II. pH effects on corrosion stability and the mechanism of coloration and bleaching. *J. Electrochem. Soc.* 126, 742–750.
- Hofer, E., Urban, G., Spach, M.S., Schafferhofer, I., Mohr, G., Platzer, D., 1994. Measuring activation patterns of the heart at a microscopic size scale with thin-film sensors. *Am. J. Physiol., 266 (Heart Circul. Physiol., 35)*, H2136–H2145.
- Kléber, A.G., Fleischhauer, J., Cascio, W.E., 1995. Ischemia-induced propagation failure in the heart. In: Jalife, J., Zipes, D. (Eds.), *Clinical Electrophysiology: From the Cell to the Bedside*. WB Saunders Co., pp. 174–182.
- Kléber, A.G., Riegger, C.B., 1987. Electrical constants of arterially perfused rabbit papillary muscle. *J. Physiol.* 385, 307–324.
- Mastrototaro, J.J., Massoud, H.Z., Pilkington, T.C., Raymond, E.I., 1992. Rigid and flexible thin-film multielectrode arrays for transmural cardiac recording. *IEEE Trans. Biomed. Eng.* 39, 271–279.
- Najafi, K., 1994. Solid-state microsensors for cortical nerve recordings. *IEEE Eng. Med. Biol. Mag.* 13, 375–387.
- Robblee, L.S., Rose, T.L., 1990. Electrochemical guidelines for selection of protocols and electrode materials for neural stimulation. In: Agnew, W.F., McCreery, D.B. (Eds.), *Neural Prostheses*. Prentice Hall, pp. 26–66.
- Smith, W.T., Brosnan, D.B., Nagle, H.T., Yang, H., Johnson, T.A., Cascio, W.E., 1996. Novel extracellular microelectrodes with high spatial resolution show variations in intramural longitudinal conduction in ischemic papillary muscles. In: Proceedings of the 40th Annual Meeting on Biophys. J., Baltimore, MD, 70, p. A278.
- Vukovic, M., 1987. Oxygen evolution reaction on thermally treated iridium oxide films. *J. Appl. Electrochem.* 17, 737–745.
- Wightman, R.M., Wipf, D.O., 1989. Voltammetry at ultramicroelectrodes. In: Bard, A.J. (Ed.), *Electroanalytical Chemistry: A Series of Advances*, vol. 15. Marcel Dekker, Inc., pp. 267–353.
- Weiland, J.D., Anderson, D.J., 2000. Chronic neural stimulation with thin-film, iridium oxide electrodes. *IEEE Trans. Biomed. Eng.* 47, 911–918.
- Zerbino, J.O., de Tacconi, N.R., Arvia, A.J., 1978. The activation and deactivation of iridium electrodes in acid electrolytes. *J. Electrochem. Soc.* 125, 1266–1276.